ACSNANO
www.acsnano.org
ARTICLE

Enhanced Li–S Batteries Using Amine-Functionalized Carbon Nanotubes in the Cathode

Lin Ma,[†] Houlong L. Zhuang,[†] Shuya Wei,[‡] Kenville E. Hendrickson,[‡] Mun Sek Kim,[‡] Gil Cohn,[‡] Richard G. Hennig,[†] and Lynden A. Archer*[,‡]

[†]Department of Materials Science & Engineering and [‡]Department of Chemical and Biomolecular Engineering, Cornell University, Ithaca, New York 14853, United States

Supporting Information

ABSTRACT: The rechargeable lithium–sulfur (Li–S) battery is an attractive platform for high-energy, low-cost electrochemical energy storage. Practical Li–S cells are limited by several fundamental issues, including the low conductivity of sulfur and its reduction compounds with Li and the dissolution of long-chain lithium polysulfides (LiPS) into the electrolyte. We report on an approach that allows high-performance sulfur–carbon cathodes to be designed based on tethering polyethylenimine (PEI) polymers bearing large numbers of amine groups in every molecular unit to hydroxyl- and carboxyl-functionalized multiwall carbon nanotubes. Significantly, for the first time we show by means of direct dissolution kinetics measurements that the incorporation of CNT-PEI hybrids in a sulfur cathode stabilizes the cathode by both kinetic and thermodynamic processes. Composite sulfur cathodes based the CNT-PEI hybrids display high capacity at both low and high current rates, with capacity retention rates exceeding 90%. The attractive electrochemical performance of the materials is shown by means of DFT calculations and physical analysis to originate from three principal sources: (i) specific and strong interaction between sulfur species and amine groups in PEI; (ii) an interconnected conductive CNT substrate; and (iii) the combination of physical and thermal sequestration of LiPS provided by the CNT=PEI composite.

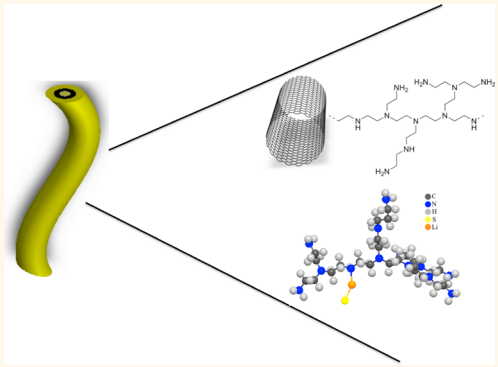

KEYWORDS: *lithium–sulfur batteries, molecular sorbents, lithium–nitrile interactions, sequestering lithium polysulfide*

The rechargeable lithium–sulfur (Li–S) battery is under active consideration by research teams worldwide as an attractive platform for high-energy, low-cost electrochemical energy.[1,2] The low cost of sulfur ($0.02/g) and the high theoretical energy density (2500 Wh/kg or 2800 Wh/L) of the sulfur cathode are widely regarded as the main drivers for this interest.[3−5] Realization of this promise in a practical Li–S cell has so far been elusive because the electrode kinetics, active material utilization, and lifetime of the cell are limited by several fundamental issues, which derive from the complex solid-state and solution physical chemistry of the electrodes and electrolyte.[6,7] The poor ionic and electronic conductivity of sulfur and its reduction compounds with lithium leads to sluggish electrode kinetics, poor active material utilization, and unacceptable overall cell performance at moderate charge/discharge rates. Dissolution of long-chain lithium polysulfides (Li_2S_x, $2 < x < 8$) (LiPS) into the electrolyte and the shuttling of polysulfides between cathode and anode consume the active material in a parasitic process that ultimately ends in premature cell failure.[8,9] Great efforts have been applied to enhance the electronic conductivity of the composite cathode and to prevent the dissolution of LiPS, the most effective of which focus on synergetic benefits of nanoengineered carbons, including micro/mesoporous carbon,[10,11] carbon nanotubes/nanofibers,[12,13] graphene/graphene oxide sheets,[14,15] and carbon nanospheres,[16,17] to simultaneously facilitate electron transport and sequester soluble species in the cathode.

Among nanoengineered carbons, carbon nanotubes (CNTs) are emerging as among the most effective and practical choices as conductivity aids in a battery cathode. In the specific case of the Li–S cell, CNTs offer at least four specific features that justify this interest: (i) CNTs have high aspect ratios, high surface area, and large surface to volume ratios. This means that their percolation threshold is low and that diffusion lengths for both lithium ions and electrons are low. The materials can therefore be thought to provide an ideally, interconnected

Received: October 9, 2015
Accepted: December 4, 2015
Published: December 4, 2015

DOI: 10.1021/acsnano.5b06373
ACS Nano 2016, 10, 1050–1059

conductive scaffold to accommodate sulfur and its poorly conductive reduction products in the cathode.[18,19] (ii) The CNT microstructure may also be beneficial for kinetically trapping long-chain LiPS in the cathode, which without compromising interfacial contact between the active materials and electrolyte limits LiPS dissolution and loss to the electrolyte.[20,21] (iii) At CNT concentrations above the percolation threshold, it creates a mechanically strong conductive scaffold in the cathode. Integration of a polymer binder and sulfur creates a mechanically robust electrode, able to accommodate periodic volume expansion and contraction of sulfur that accompanies its redox reaction with lithium.[12,19] (iv) With worldwide efforts focused on economical processes for large-scale and cost-effective manufacture of CNTs, a variety of CNTs are now available at modest prices of $0.10−25/g. It is predicted that this cost could drop to as little as $10−30/kg within the next 10 years, when production capacity is expected to reach hundreds of thousand of tons annually.[22]

The barriers CNTs and other carbon-based nanomaterials present to dissolution of LiPS are now understood to be kinetic; a soluble LiPS species physically trapped by the host material will eventually leach into the electrolyte. It is possible to augment interactions between cathode components and LiPS by using polar additives or metal oxides such as SiO_2,[23] TiO_2,[24] and Al_2O_3.[25] The strong affinity between LiPS and nitrile- or chlorine-containing molecules has recently been confirmed by both density functional theory and diffusion experiments.[26] Oxides are also applied to serve as polysulfide reservoirs to hinder the dissolution of sulfur species. Polymer coatings have already been used as an additional physical barrier to hinder LiPS dissolution; however these barriers are insufficient for at least two reasons. First, they only reduce the kinetics of LiPS loss to the electrolyte, which makes their effect temporary. Second, the conductivity of the electrode is decreased as a result of the insulating polymers typically employed.[21,27] Another approach is to modify the carbon surface with amphiphilic polymers to improve the interaction. Polyvinyl pyrollidone (PVP), for example, has been employed in this manner as a coating onto a carbon surface *via* nonpolar physical adsorption.[28] However, the modification is just a physical wrapping/coating of the carbon/sulfur particles; thus the effect will fade with time when there is no bonding between those polymers and the carbon substrate. A big disadvantage of all these methods is that the polar additives or oxides or the polymer coatings are insulators, which will lower the conductivity of the electrode, resulting in limited utilization of the active materials.

Here we report an approach that allows high-performance sulfur−carbon composite cathodes to be designed and synthesized. Specifically, hybrid particles composed of multiwall carbon nanotubes covalently grafted with polyethylenimine (PEI) polymers, bearing a large amount of amine groups in every molecular unit, are created *via* a grafting-to reaction using hydroxyl and carboxyl groups on the CNTs. The hybrid particles are shown to form effective anchors for LiPS in the Li−S battery cathode. Covalent attachment of PEI to CNT is confirmed by XPS and Raman spectroscopy. In addition, the strong affinity of LiPS to PEI-functionalized CNTs is verified by density-functional theory (DFT) calculations, which yield a substantial binding energy of 1.24 eV. Significantly, we show *via* direct dissolution kinetics measurements that incorporation of the hybrids in the sulfur cathode produces a factor of 3 or more reduction in the dissolution rate and equilibrium concentration of LiPS in the electrolyte. These features together with other intrinsic merits of CNTs, such as effective physical trapping for LiPS,[19−21] good conductivity, and robust mechanical properties, are shown to yield CNT-PEI/sulfur composite cathodes that exhibit excellent electrochemical properties, including stable cycling performance at rates up to 3.35 mA/cm^2 or 2C.

An advantage of our materials design is that we are able create strong and multidentate interactions with LiPS and elemental sulfur throughout the cathode. This means that the content of PEI need not be large; for the present study it never exceeded 8%, compared with ∼20% in typical coating studies.[21,27] A second advantage comes from the fact that the PEI is covalently bonded to the cathode substrate, through strong, but sparse amide linkages. This means that the electrode architecture is preserved under the mechanical and chemical stresses that accompany extended cycling. The sparse covalent attachment of PEI is also beneficial, as it allows the high electrical conductivity of the electrode to be preserved.

RESULTS AND DISCUSSION

Scheme 1 illustrates the two-step preparation procedure of the CNT-PEI/sulfur composite: First, PEI is covalently attached to

Scheme 1. Schematic of Procedure for Preparing CNT-PEIS Nanocomposites

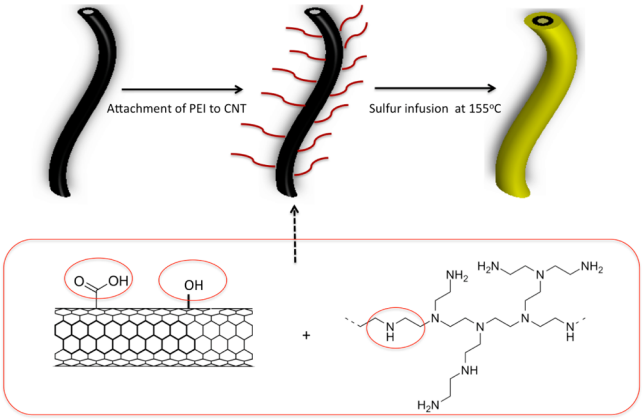

the CNTs *via* a reaction with the hydroxyl and carboxyl functional groups on the CNTs. The reaction product is vigorously washed with water to remove any excess PEI, which is highly soluble in water, and dried in preparation for the next step. In the second step, sulfur is loaded to the composite by liquid infusion and annealing at 155 °C, the temperature at which liquid sulfur has its lowest viscosity.[29] Multiple analytical tools were used to verify the covalent attachment of PEI to the CNTs and to characterize the interaction between PEI and the discharge products in the sulfur cathode. The X-ray photoelectron spectroscopy (XPS) survey scanning spectra are presented in Figure 1a and b. It is apparent that before reaction with PEI there is a signal only from C 1s (285 eV) and O 1s (532 eV), which arises from the hydroxyl and carboxyl groups on the CNTs. After reaction with PEI and washing to remove the untethered PEI, there is an additional N 1s signal (400 eV), providing evidence that the PEI is bonded to the CNT substrate. Deconvolution of the N 1s signal reveals peaks for both amine (399.3 eV) and amide (401.8 eV) groups, implying that bonding between PEI and carboxylic acid groups on the particles has occurred and that, even after attachment to CNT, amine groups remain available for interaction with LiPS.

DOI: 10.1021/acsnano.5b06373
ACS Nano 2016, 10, 1050−1059

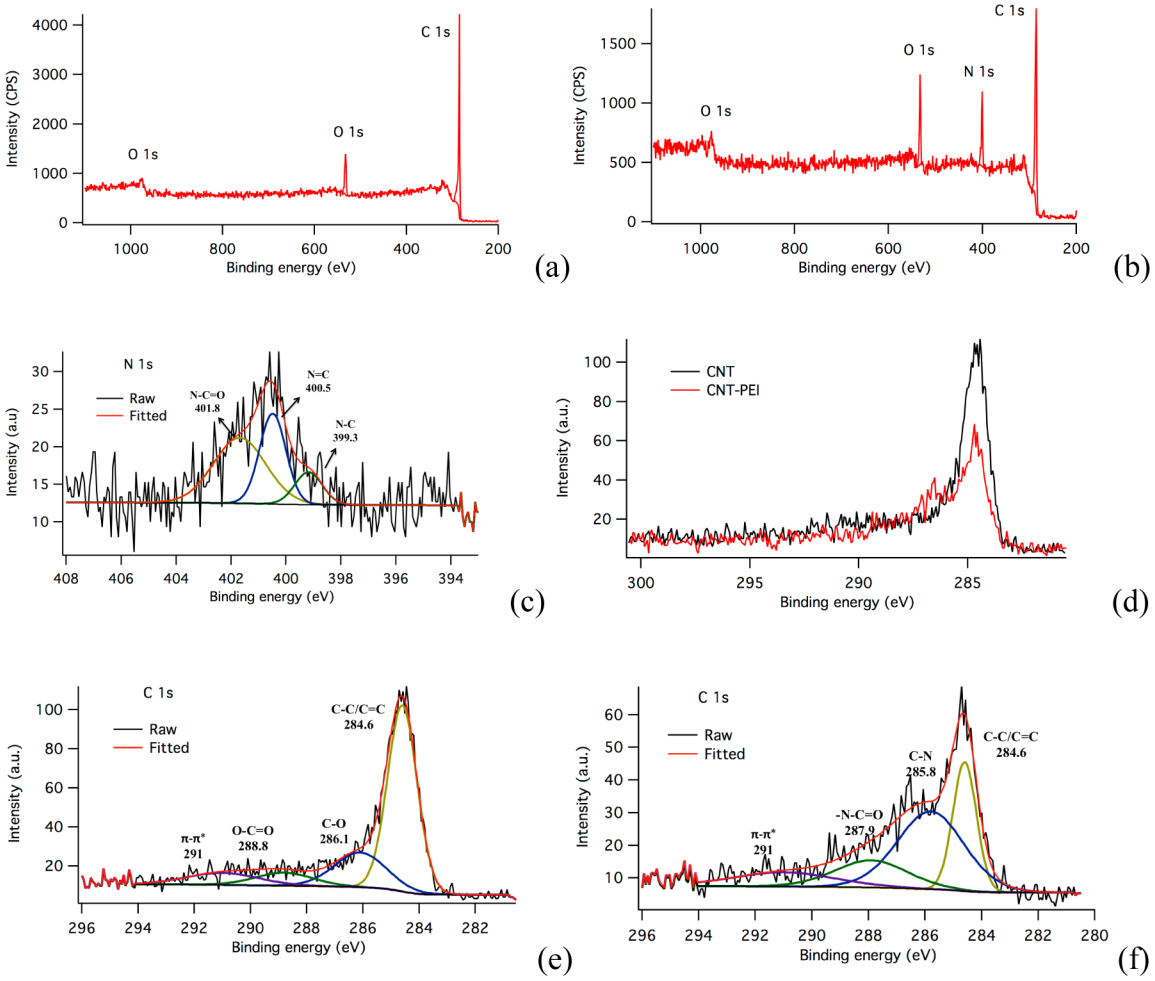

Figure 1. XPS survey scanning spectra for (a) unmodified CNTs and (b) PEI-modified CNTs. (c) High-resolution N 1s spectrum of PEI-modified CNTs. (d) Comparison of the C 1s signal of CNTs before and after attachment of PEI. (e) High-resolution C 1s XPS spectrum of unmodified CNTs. (f) High-resolution C 1s XPS spectrum of PEI-modified CNTs. (f) High-resolution C 1s XPS spectrum of PEI-modified CNTs.

Besides the N signal, the C 1s signal is also altered after reacting PEI and CNTs (Figure 1d). Before the PEI treatment, the C 1s spectrum shows the C−O hydroxyl bonding at 286.1 eV and O−C═O carboxyl bonding at 288.8 eV (Figure 1e).[30,31] After the reaction with PEI, signals associated with the C−N amine bond at 285.6 and −N−C═O bonding at 287.9 eV appear.[32,33] Furthermore, the hydroxyl and carboxyl bonding signals disappear, indicating the nearly complete conversion of hydroxyl and carboxyl groups (Figure 1f).

Density functional theoretical analysis was used to quantify the strength of the interactions between PEI and LiPS. The Gausian09 program using the PBE exchange−correlation functional and cc-pVDZ basis sets was used for this analysis. The optimized atomic configuration of LiPS and PEI is illustrated in Figure 2a. This analysis also reveals a high binding energy of 1.24 eV, which is significantly higher than the binding energy (0.34 eV) between LiPS and graphene;[28] it is also higher than that of 0.83 eV, between LiPS and poly(vinylidene difluoride) (PVDF),[34] a common binder for the sulfur cathode. The DFT analysis can be used to calculate the IR spectra of PEI and for LiPS/PEI mixtures. Figure 2b compares the calculated spectra for pure PEI and a LiPS/PEI mixture. An additional infrared peak at 640 cm^{-1} in the mixture of PEI and LiPS is apparent. The analysis further shows that this peak results from the formation of N−Li bonds in the mixtures.[35] Experimental FTIR spectra for pure PEI and mixture of LiPS and PEI are reported in Figure 2c and d, respectively. A distinct, but weak peak appears at around 650 cm^{-1} in the spectrum for LiPS/PEI, but is not seen in pure PEI. We view this as confirmation of the DFT result and supportive of the formation of Li−N bonds in the composites. Further, the peak at around 3200 cm^{-1} corresponding to the N−H stretching mode shifts to a lower number in the mixture compared to pure PEI. More importantly, this shift is not observed for any of the other vibration modes, such as the one associated with the CH_2 bend at 1455 cm^{-1} (Figure 2d).

The bonding between the amine groups and the LiPS is also verified by the XPS spectra of the discharge product of the sulfur/PEI-CNT composite cathodes. The Li 1s spectrum (Figure 3a) shows a Li−N and a Li−S signal, which is in agreement with expectations for formation of a Li−N bond.[36] The N 1s spectrum is also changed after discharge, indicating the interaction again in a manner consistent with the presence of strong interactions between LiPS cathode discharge products and amine groups present in the cathode (Figure 3b).

The XPS S 2p spectrum of the composite shows the successful loading of sulfur onto the CNTs (Figure 3c). The S 2p signal can be deconvoluted into an S $2p_{3/2}$ and $2p_{1/2}$ doublet

DOI: 10.1021/acsnano.5b06373
ACS Nano 2016, 10, 1050−1059

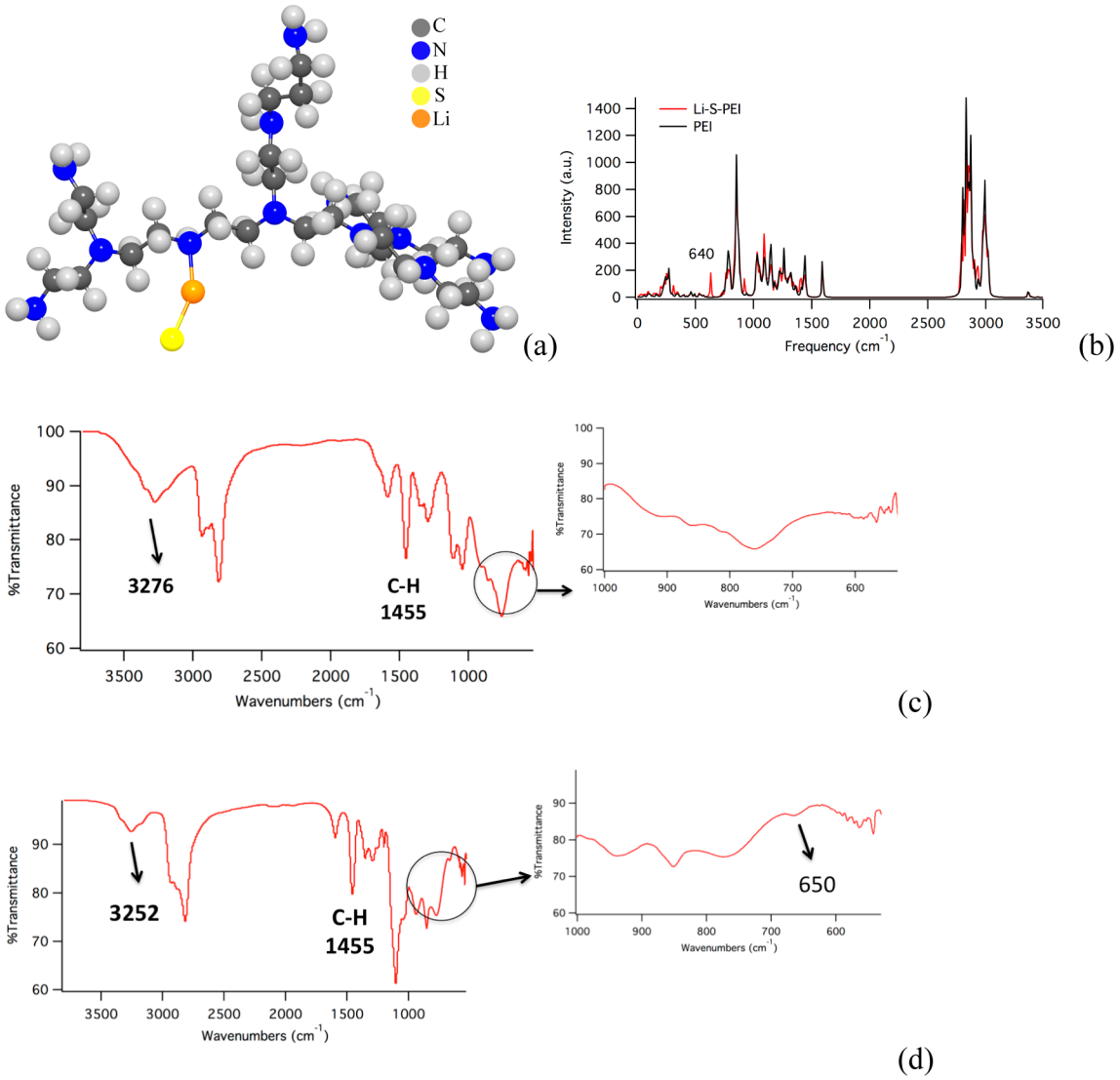

Figure 2. (a) Structure of PEI deduced from DFT analysis of the binding energy between PEI and the Li−S· species. (b) DFT calculation of IR spectra of the mixture of Li−S· species and PEI (red) and pure PEI (black). (c) Experimental FTIR spectra of pure PEI. (d) Experimental FTIR spectra of a mixture of Li_2S_9 and PEI.

at 163.8 and 165 eV, respectively, with the expected energy separation of 1.2 eV and intensity ratio of 2:1.[37,38] The binding energy of the S $2p_{3/2}$ peak is slightly lower than the literature value, and this happens after the calibration of the C−C peak to 284.6 eV, implying that elemental sulfur interacts with the composite. In the S 2p signal after discharge, lithium sulfide peaks are observed between 161.5 and 162.7 eV,[36,39] indicating the full discharge of elemental sulfur. There is also a sulfate signal, which is thought to result from the air and moisture sensitivity of Li_2S. To probe the interaction between the amine group on PEI and sulfur upon sulfur loading, a high-resolution scan of the N spectrum before and after sulfur loading was performed. The results reported in Figure 3d and e show that the area of the peak corresponding to the amine group decreases, strongly indicative of a chemical reaction at the amine group. Previous studies have reported that sulfur mixed with amine-containing organic molecules results in the formation of compounds with sulfur−amine bonds.[39−41] The amine group donates an electron to elemental sulfur, leading to a decrease of amine group content detected by XPS. This reaction also explains why the sulfur peaks shift to lower binding energy: the electron donation from the amine groups enhances the electric field, reducing the energy for the S 2p electron to be knocked out by the X-rays.

The Raman spectra of the composite also provide information about the interaction between elemental sulfur and the CNT-PEI composite (Figure 4 and Table 1). The intensity ratio between the D band (I_D) and the G band (I_G) is indicative of a basic structural change in the CNTs, with a greater value of this parameter implying more defects.[42,43] Upon sulfur loading onto the CNT composite, an increase in the I_D/I_G ratio is observed, indicating an increase of sp^3 carbons on the nanotubes, which implies that sulfur interrupts the C═C sp^2 bond in CNTs. Thus, both XPS and Raman spectra verified that sulfur is anchored to the composite *via* strong chemical interaction.

Two CNT-PEI/S composites, CPS-59 and CPS-70, with different sulfur content (59 and 70 wt %, respectively) were prepared, and the sulfur content determined the use of thermogravimetric analysis (TGA) (Figure S1) as described in the Supporting Information. Table S1 summarizes the surface area and pore size information derived from Brunauer−

DOI: 10.1021/acsnano.5b06373
ACS Nano 2016, 10, 1050−1059

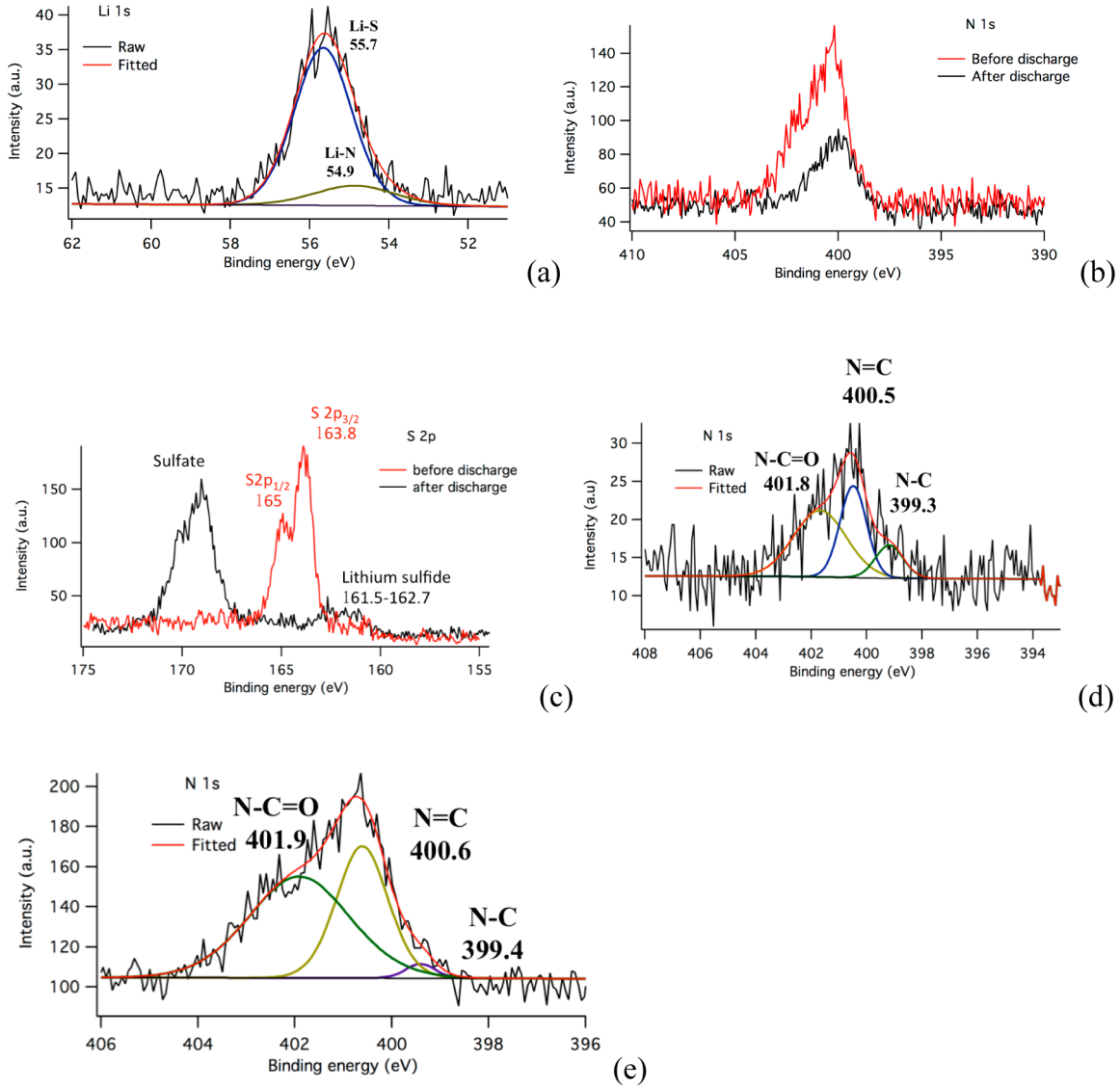

Figure 3. High-resolution XPS spectra for (a) Li 1s of the discharge product of the CNT-PEIS composite; (b) N 1s before and after discharge; (c) S 2p before and after discharge; (d) N 1s of the CNT-PEI composite before sulfur loading; and (e) N 1s of the sulfur-loaded CNT-PEI composite.

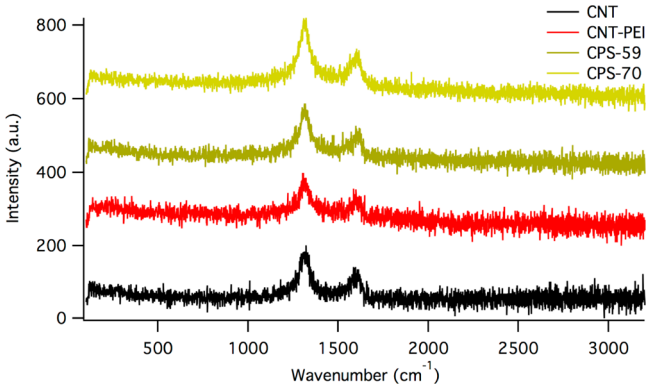

Figure 4. Raman spectra of CNT, CNT-PEI, and the sulfur-loaded CNT-PEI composite.

Emmett−Teller (BET) analysis. Upon sulfur loading, with the infusion of the sulfur in the microstructure provided by the CNT network, the pore volume and pore size of the composite decrease, and the effect is even more dramatic when higher sulfur content is loaded. These results indicate that the sulfur is filled in the microstructure of CNTs, while still allowing electrolyte access to the active materials by the presence of residual micropores. X-ray diffractometer (XRD) analysis of CNT-PEI and CNT-PEI/S composites (Figure 5) was used to probe the crystal structure of the materials. The attachment of PEI onto CNTs clearly does not affect the carbon structure, but the sulfur spectrum is affected by sulfur loading in the composites. At 59 wt % sulfur, only a weak sulfur peak is observed, which implies that sulfur is mostly amorphous. In contrast, at 70 wt % sulfur, there is a strong peak associated

Table 1. Raman I_D/I_G Ratio for Different Nanocomposites

	I_D/I_G
CNT	1.94
CNT-PEI	2.02
CPS-59	2.34
CPS-70	2.47

DOI: 10.1021/acsnano.5b06373
ACS Nano 2016, 10, 1050−1059

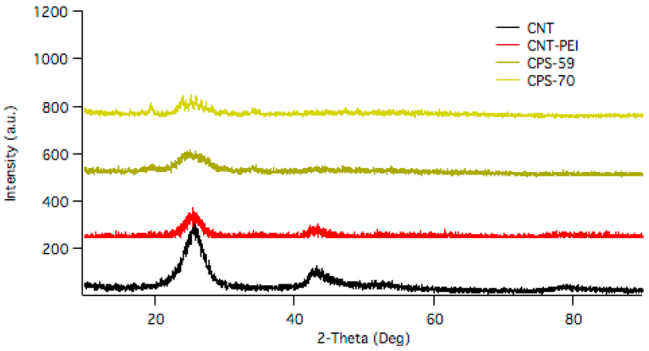

Figure 5. XRD angle-dependent intensity profiles for CNT-PEI and CNT-PEI/S nanocomposites with different sulfur loadings.

with crystalline sulfur. The loss of crystallinity of sulfur in the composites at the lower sulfur loading can be interpreted in terms of the confinement of sulfur in the cathode associated with its interactions with the CNT-tethered PEI. At the higher sulfur loading, we believe that all of the sulfur is not anchored to PEI and as such is freer to adopt crystalline structures typical of the equilibrated material so that the crystal structure can be detected by XRD. This interpretation is consistent with the observation of a sulfur loss process at elevated temperature in TGA experiments using composites with 59 wt % sulfur. Figure S2 compares the impedance of Li−S cells using cathodes composed of a physical mixture of carbon black and sulfur (70 wt %), CNTS-60, CPS-59, and CPS-70. The impedance is observed to decrease dramatically for all of the CNT-based materials. Also, at the same sulfur loading, the impedance of the CNT-PEI/S composite is comparable or even smaller than that of CNT-60, implying that the attachment of PEI not only maintained the high conductivity of CNT matrix but also improved it to some extent, perhaps because the oxygen-containing functional groups on CNT are replaced. In contrast, in previous studies employing polymer coatings in sulfur cathodes,[21,27] the insulating polymer adsorbs indiscriminately on the conductive surfaces in the electrode, increasing the resistance at the electrolyte/electrode interface, which limits the rate capability of the cathode.

The covalent attachment of PEI onto CNTs and the affinity of LiPS for PEI-functionalized CNTs implies that Li/S battery cathodes based on the materials should exhibit improved performance upon extended electrochemical cycling. Figure 6a reports results from cyclic voltammetry (CV) of Li/S cells using CPS-70 as a cathode, with a scanning rate of 0.1 mV/s. During discharge/charge process, a pair of redox peaks is observed at potentials consistent with the two stages of reduction and oxidation of sulfur. The stable position and intensity of the peaks demonstrate the steady and reversible electrochemical reaction of sulfur in the composite. Similarly, the voltage profile obtained from galvanostatic discharge experiments at 838 mA/g (0.5C, based on the theoretical capacity of sulfur) reported in Figure 6b shows two strong voltage plateaus over many cycles. The first discharge plateau at ∼2.35 V corresponds to the reduction of elemental sulfur into high-order LiPS. The second plateau at ∼2.0 V is indicative of the reduction of high-order LiPS into low-order LiPS. Figure 6c compares the long-term cycling performance of Li−S batteries with three different types of cathodes, a CNT-PEI composite with 59 wt % sulfur content (CPS-59), a CNT-PEI composite with 70 wt % sulfur content (CPS-70), and unmodified CNTs with 60% sulfur content (CNTS-60), but with the same sulfur infusion treatment, cycled galvanostatically at 0.5C. There is very obvious improvement in performance of cathodes based on the CNT-PEI hybrids. The capacity of the unmodified CNT is seen to fade quickly, consistent with loss of active materials from the carbon matrix, while the performance of the sulfur-loaded CNT-PEI composite is very stable with high Coulombic efficiency. In a conventional Li−S battery, a high initial capacity loss is typically observed due to the dissolution of LiPS. Once in the electrolyte, the LiPS cannot be fully recovered in the following charge process, which leads to poor utiliztion of the active electrode material and capacity fading.[21,26,43] In lithium−sulfur cells employing CNT-PEI/S composites, it is apparent that very stable performance is observed, even at 70% sulfur content. These performance improvements evidently stem from PEI's role in effectively preventing LiPS dissolution and the intrinsic improvements in cathode conductivity stemming from the CNT substrate. It is also apparent that the initial capacity of Li−S cells employing the CNT-PEI/S composites is slightly lower than the typical value;[23,26] this result is thought to be due to the need for an activation process over the first few cycles since elemental sulfur is strongly interacting with the composite. Interestingly, CPS-70 exhibits higher electrochemical energy storage capacity than CPS-59, while the cycling performance of CPS-59 is more stable than that of CPS-70. These differences can be explained in terms of differences in the features observed in XRD and TGA analysis of the composites. CPS-70 has higher sulfur content and shows strong crystalline sulfur peaks in the XRD, indicating part of the sulfur is not anchored to the CNT, which might be responsible for the capacity fading in CPS-70 since the exposed sulfur will be dissolved into the electrolyte upon sulfur reduction. In contrast, in CPS-59, the sulfur is mostly confined and anchored onto the composite; thus very little capacity fading is observed in the cycling performance. After deep cycling of the CPS-70 electrode for as many as 300 cycles at 0.5C, a high capacity of 750 mAh/g can be retained, corresponding to a high capacity retention of ∼79% (Figure 6d). The simultaneous achievement of exceptional cycling stability and nearly 100% Coulombic efficiency over 300 cycles seen in Figure 6d also provides strong support for the suppression of the shuttling of LiPS in Li−S cells utilizing CNT-PEI/S composites as cathodes.

High rate capability of the CNT-PEIS composite is shown in Figure 6e, where CPS-70 is cycled at 1C (1675 mA/g) and 2C (3350 mA/g). The capacity of the cells generally follows the typical trend that at a lower current rate the capacity is higher. The cycling stability at 0.5C is better than 1C and 2C, but it is comparable at 1C and 2C after the capacity reaches steady state. Figure 6g shows the excellent rate capabilities of CPS-70 at various current densities, where the capacity of CPS-70 can recover to high values at 0.5C after high current (4C) is applied.

To develop a deeper understanding of the working mechanism of the CNT-PEI/S composites, the morphology of the materials before and after discharge was interrogated using scanning electron microscopy (SEM) (Figure 7). Figure 7a and b show that the attachment of PEI to CNTs has no observable effect on the morphology of the CNTs. In contrast, Figure 7c and d show that the CNT-PEI/S composites with different sulfur loadings have very different morphologies. In particular, for CPS-70, sulfur particles are observed on the surface of the material, while almost none are seen for CPS-59. This observation explains the difference observed in the XRD

DOI: 10.1021/acsnano.5b06373
ACS Nano 2016, 10, 1050−1059

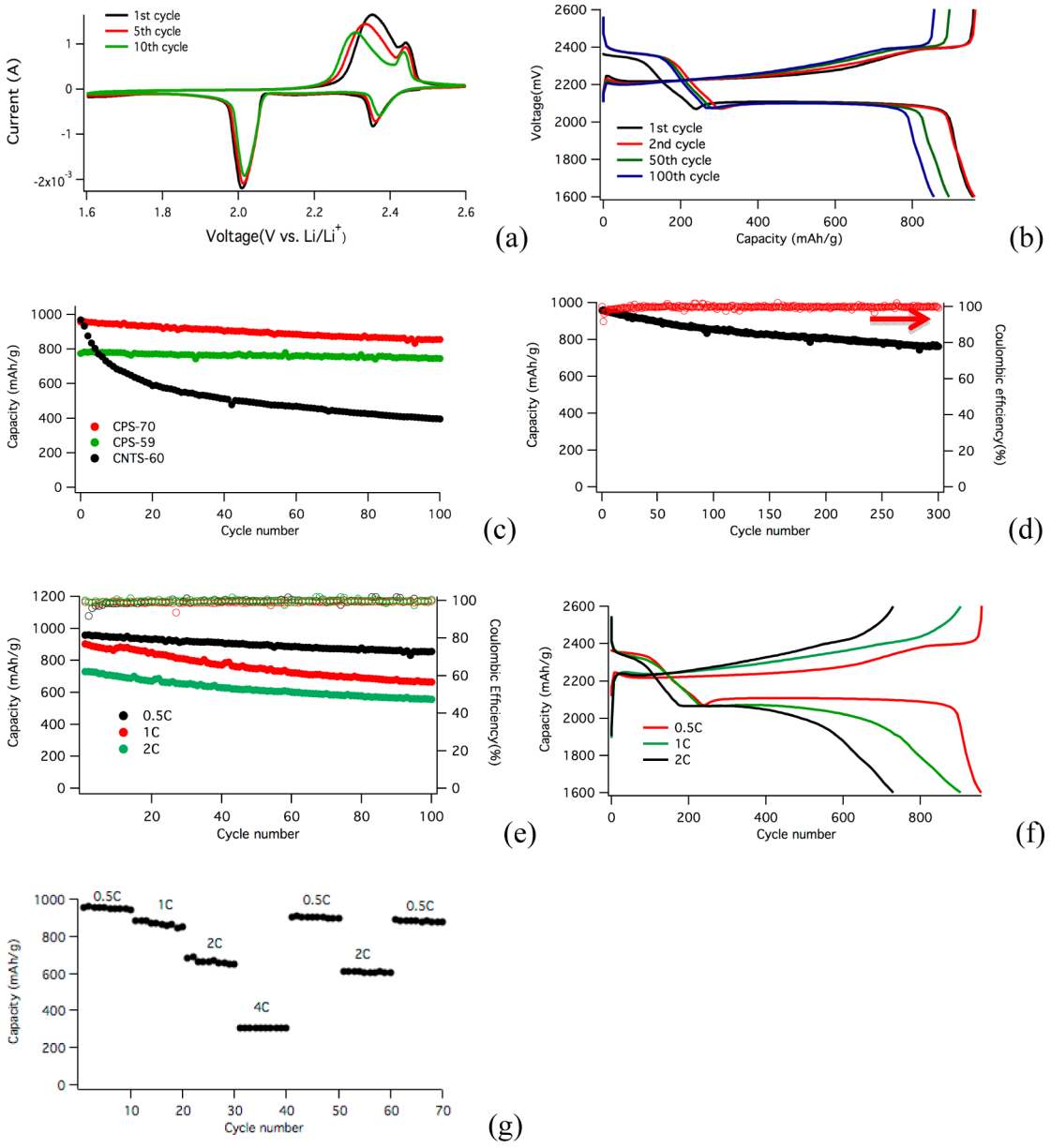

Figure 6. (a) Cyclic voltammogram for a Li−S cell containing CPS-70 as cathode at a fixed scan rate of 0.1 mV/s. (b) Voltage *vs* capacity plot at different cycles for a Li−S cell with CPS-70 as cathode cycled at 0.5C (838 mA/g). (c) Long-term cycling performance of Li−S cells with CPS-70, CPS-59, and CNTS-60 as cathodes, respectively, cycled at 0.5C (838 mA/g). (d) Capacity and Coulombic efficiency for Li−S cells based on CPS-70 cathodes subjected to deep cycling at 0.5C (838 mA/g). (e) Long-term cycling performance of Li−S cells with CPS-70 cycled at 0.5C (838 mA/g), 1C (1675 mA/g), and 2C (3350 mA/g), respectively, with solid circles representing capacity and blank circles representing Coulombic efficiency. (f) Voltage *vs* capacity profile for a Li−S cell with CPS-70 as cathode cycled at 0.5C (838 mA/g), 1C (1675 mA/g), and 2C (3350 mA/g), respectively. (g) Rate capabilities of CPS-70 at various current densities.

spectra and cycling performance between the two materials; only a fraction of the sulfur is anchored to the CNT-PEI hybrids in the cathode. Figure S4 reports the elemental mapping of carbon and sulfur in CPS-59 within the selected area, indicating a homogeneous distribution of carbon and sulfur in the composite. The morphology of the composite after discharge is reported in Figure 7e−g, showing that the unmodified CNT is coated with a large and nonuniform Li_2S particle/layer after discharge, while for the CNT-PEI, the morphology of the CNTs is still maintained after the discharge. This difference is likely a reflection of the strong affinity between PEI and LiPS, which can help to anchor both the elemental sulfur and the reduction products to prevent their detachment from both the inner and outer surface of the CNT.

As a final step to understanding the superior electrochemical behaviors of the CNT-PEI/S composite cathodes, we directly evaluate the dissolution kinetics of LiPS trapped in the cathode. Electrode coupons composed of LiPS composited with the different types of carbon matrices (unmodified CNT and the CNT-PEI composite) were immersed into 10 mL of tetraglyme, a good solvent for LiPS and a commonly used electrolyte solvent in Li−S cells, and the time-dependent concentration of the solution was measured (Figure S5). The solvent was continuously stirred during the measurements to ensure uniform distribution of sulfur species in the electrolyte,

DOI: 10.1021/acsnano.5b06373
ACS Nano 2016, 10, 1050−1059

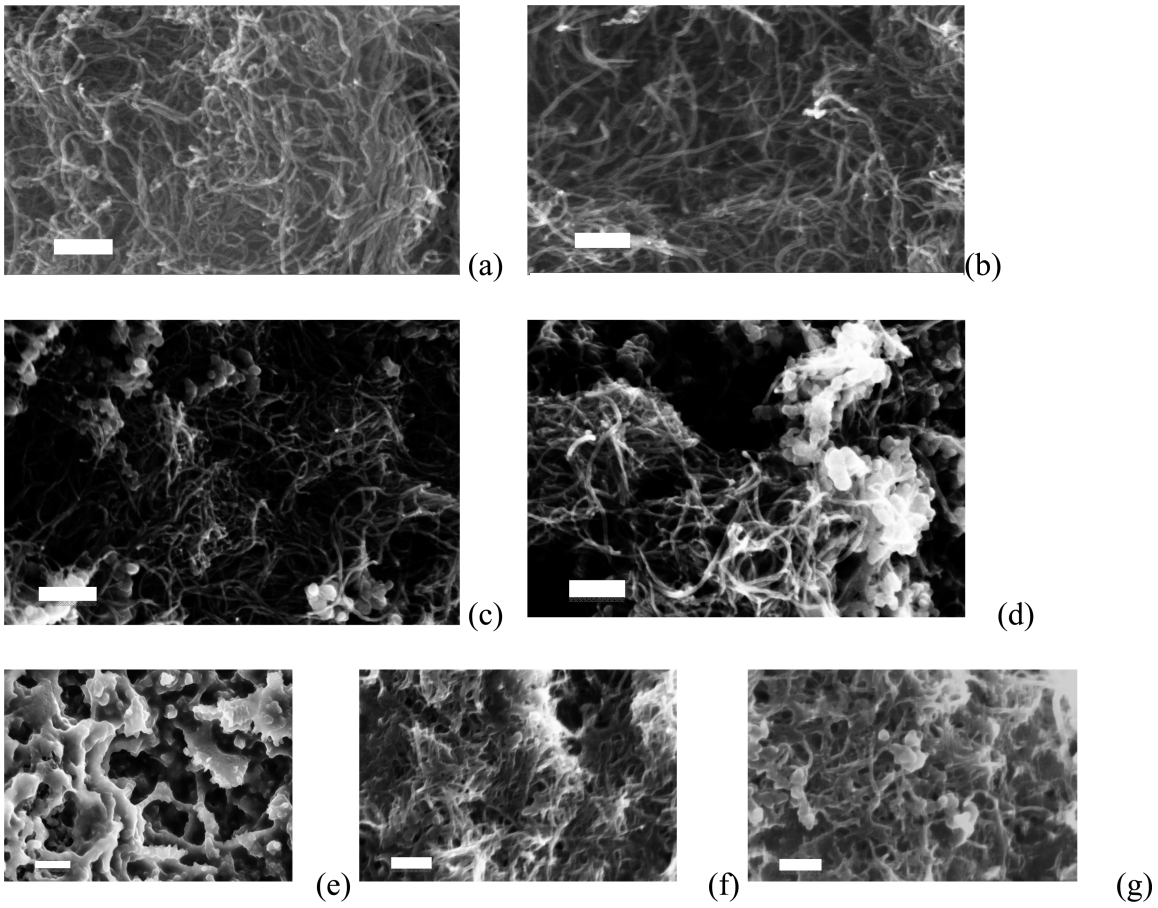

Figure 7. SEM images for (a) pristine CNT; (b) CNT-PEI hybrid; (c) CPS-59; (d) CPS-70; (e) Li−S cell cathode using CNT/S-60 after discharge; (f) Li−S cell cathode applying CPS-59 after discharge; and (g) Li−S cell cathode applying CPS-70 after discharge. Scale bar = 200 nm.

allowing the sulfur concentration at different times to be determined by inductively coupled plasma atomic emission spectroscopy (ICP-AES) (Figure S6), performed on small aliquots of the extracted electrolyte. The rate constant k for dissolution can be determined from the time-dependent concentration information, with the help of eqs 1−3. Specifically, a straight line plot of $\log_e(1 - c/c_s)$ *vs* time yields k as the slope. This analysis also yields the equilibrium concentration (c_s) of LiPS in the electrolyte, at which LiPS has equal chemical potential in the electrolyte and cathode. Comparing dissolution rate constants in each case (Table 2), the CNT-PEI is seen to reduce the rate of dissolution of LiPS by a factor of 3 or more. Additionally, Table 2 shows similar large reductions in c_s and percentage LiPS loss to the electrolyte at steady state, supporting our hypothesis that the changes are thermodynamic and the anchoring of sulfur to the CNT-PEI support is covalent. It is also apparent that both the solubility and dissolution rates are higher with increasing chain length of LiPS (Table 2).

Table 2. Rate Constant for Dissolution k, Percentage of Loss of Sulfur into the Electrolyte, and Equilibrium Concentration c_s in Each Case

	k	loss of sulfur in the electrolyte (%)	c_s (mg/L)
Li_2S_9 with CNT	6.22×10^{-5}	78	2300
Li_2S_4 with CNT	6.1×10^{-5}	39	1172
Li_2S_9 with CNT-PEI	2.1×10^{-5}	16	481
Li_2S_4 with CNT-PEI	1.16×10^{-5}	12	350

$$dc/dt = k(c_s - c) \quad (1)$$

$$c = c_s(1 - e^{-kt}) \quad (2)$$

$$-kt = \log_e(1 - c/c_s) \quad (3)$$

where k is the rate constant of dissolution, t is time, c is concentration of LiPS dissolved into the electrolyte, and c_s is equilibrium concentration.

CONCLUSIONS

In summary, we have reported a procedure for creating multiwall carbon nanotube−polyethylenimine hybrid particles as a platform for thermally sequestering lithium polysulfides in the sulfur cathode of a Li−S cell. By means of spectroscopic analysis we show that the PEI is covalently linked to the CNT. By means of density functional theoretical analysis and spectroscopic measurements we further show that the large number of amine groups present in each PEI chain produces strong, covalent-like bonding of LiPS in the cathode. Direct measurements of the dissolution kinetics of LiPS/CNT and LiPS/CNT-PEI composites in tetraglyme show that both the dissolution rate and equilibrium concentration of LiPS in the

DOI: 10.1021/acsnano.5b06373
ACS Nano 2016, 10, 1050−1059

electrolyte are substantially lower for the CNT-PEI materials, indicating that they stabilize the sulfur cathode by a combination of kinetic and thermodynamic means. Application of the materials as cathodes in Li−S batteries provides a substantial and obvious relationship between anchoring of sulfur in the cathode and cycling performance of the cells.

MATERIALS AND METHODS

Preparation of CNT-PEI Composites. A multiwalled, carboxylic acid functionalized carbon nanotube (>8% carboxylic acid functionalized, av diam × L = 9.5 nm × 1.5 μm) was obtained from Sigma-Aldrich and was dried before use. Polyethylenimine solution (50 wt % in water) was obtained from Sigma-Aldrich (average $M_w \approx 750\,000$ by LS, average $M_n \approx 60\,000$ by GPC). The CNT-PEI composite was synthesized by heating a mixture of 100 mg of CNT suspension (1 mg/mL) and 1 g of PEI solution at 80 °C with stirring for 12 h. The product was washed with water five times and dried at 100 °C overnight.

Preparation of CPS-59, CPS-70, and CS-60. Sulfur incorporation was performed using the vapor phase infusion method. For CPS-59, mixture of sulfur and CNT-PEI composite at a weight ration of 1.5:1 is ball milled for 20 min, after which the mixture was sealed in a glass tube under vacuum. The mixture was heated at 155 °C for 6 h. CPS-70 was prepared in the same way but with a ratio of sulfur to CNT-PEI of 2.5:1. In the preparation of CS-60, unmodified CNT is used and sulfur:CNT = 1.5:1.

Preparation of Li_2S_4 and Li_2S_9 for FTIR Analysis and Dissolution Kinetics Studies. To synthesize Li_2S_4, 920 mg of Li_2S, 3.2 g of sulfur, and 0.5 g of lithium powder (from FMC Lithium) were added to 5 mL of tetraglyme (tetraethylene glycol dimethyl ether) and strirred for 24 h. The mixture was filtered to obtain a dark reddish liquid. Li_2S_9 was prepared following Rauh et al.'s procedure[44] in a solution process where stoichiometric amounts of elemental sulfur and Li_2S were codissolved into tetraglyme, followed by heating at 80 °C with stirring for 6 h.

Characterization. Interaction between PEI and LiPS was characterized using FTIR spectroscopy by using a Bruker Optics Vertex80v infrared spectrometer with air-sensitive samples tested in a vacuum-evacuated chamber. Crystal structure was characterized using a Scintag Theta−Theta X-ray diffractometer. Thermogravimetric analysis was used to determine the content of sulfur in the composite. Raman spectra was done by using a Renishaw Invia confocal Raman microscope. Morphologies of the electrodes were studied using a LEO 1550 FESEM (Keck SEM) and a FEI Tecnai G2 T12 Spirit TEM (120 kV). Impedance was measured *versus* frequency using Novocontrol N40 broadband dielectric spectroscopy. X-ray photoelectron spectroscopy is used for elemental analysis and to obtain chemical bonding information. ICP-AES was used to quantify sulfur content in the electrolytes as a function of time.

Electrochemical Characterization. A total of 2030 coin-type cells were assembled using lithium metal (0.76 mm thick, Alfa Aesar) as the anode electrode, microporous Celgard 2500 membranes as separator, a cathode with 80% as prepared C/S composite, 10% Super-P Li carbon black from TIMCAL, and 10% poly(vinylidene difluoride) (Sigma-Aldrich) as binder in an excess of *N*-methyl-2-pyrrolidone in NMP, and an electrolyte of 40 μL of 1 M lithium bis-(trifluoromethanesulfone)imide (LiTFSI) and 0.2 M $LiNO_3$ in 1,3-dioxolane/1,2-dimethoxyethane (v/v = 1:1) for each cell. The sulfur loading per electrode was 1.2 mg/cm^2. Cell assembly was carried out in an argon-filled glovebox (MBraun Labmaster). The room-temperature cycling characteristics of the cells were evaluated under galvanostatic conditions using Neware CT-3008 battery testers, and electrochemical processes in the cells were studied by cyclic voltammetry using a CHI600D potentiostat.

Preparation of LiPS Electrode for Dissolution Kinetics Studies. Li_2S_4 and Li_2S_9 were prepared as described above. A 30 mg amount of LiPS species (10 wt % in tetraglyme solution), 100 mg of CNT or CNT/PEI, and 20 mg of PVDF were mixed, coated onto alumina, and used for the kinetic study before drying under vacuum. Heat was not applied due to the unstable properties of LiPS decomposition into other forms when exposed to air or heat. All of the electrode preparation and sample collection was done in a glovebox.

Theoretical Section. We perform the DFT calculations using the Gausian09 program with the PBE exchange−correlation functional and the cc-pVDZ basis sets.[45] Similar to previous studies,[26,34] species of lithium polysulfides are modeled by Li−S dimers. All atomic coordinates are fully relaxed until the maximum interatomic forces are less than 4.5 × 10^{-4} hartree/bohr or 0.023 eV/Å. The binding energy E_b between a LiS dimer and PEI is calculated with $E_b = E_{PEI} + E_{LiS} - E_{PEI+LiS}$, where E_{PEI} denotes the total energy of a pure PEI polymer, E_{LiS} refers to the total energy of the LiS dimer, and $E_{PEI+LiS}$ is the total energy of the functionalized system.

ASSOCIATED CONTENT

Supporting Information

The Supporting Information is available free of charge on the ACS Publications website at DOI: 10.1021/acsnano.5b06373.

Additional information (PDF)

AUTHOR INFORMATION

Corresponding Author

*E-mail: laa25@cornell.edu.

Notes

The authors declare the following competing financial interest(s): Lynden Archer is a founder and holds financial interest in NOHMs Technologies, a technology company seeking to commercialize electrolytes and electrodes for high-voltage lithium ion and lithium sulfur batteries.

ACKNOWLEDGMENTS

The authors acknowledge support of the National Science Foundation Partnerships for Innovation Program (grant no. IIP-1237622). This research also used computational resources of the Texas Advanced Computing Center under contract no. TG-DMR050028N and no. TG-DMR140067. Electron microscopy, X-ray diffraction, and X-ray photoelectron spectroscopy facilities and optical spectrometers available through the Cornell Center for Materials Research (CCMR) were used for this work (NSF grant DMR-1120296).

REFERENCES

(1) Ma, L.; Hendrickson, K.; Wei, S.; Archer, L. A. Nanomaterials: Application in Lithium Sulfur Battery. *Nano Today* **2015**, *10*, 315−338.

(2) Bruce, P. G. Energy Storage Beyond the Horizon: Rechargeable Lithium Batteries. *Solid State Ionics* **2008**, *179*, 752−760.

(3) Ma, L.; Wei, S.; Zhuang, H. L.; Hendrickson, K. E.; Hennig, R. G.; Archer, L. A. Hybrid Cathode Architectures for Lithium Batteries Based on TiS_2 and Sulfur. *J. Mater. Chem. A* **2015**, *3*, 19857−19866.

(4) Wei, S.; Ma, L.; Hendrickson, K. E.; Tu, Z.; Archer, L. A. Metal-Sulfur Battery Cathodes Based on PAN-Sulfur Composites. *J. Am. Chem. Soc.* **2015**, *137*, 12143−12152.

(5) Urbonaite, S.; Poux, T.; Novák, P. Progress Towards Commercially Viable Li−S Battery Cells. *Adv. Energy Mater.* **2015**, *5*, 1500118.

(6) Evers, S.; Nazar, L. F. New Approaches for High Energy Density Lithium−Sulfur Battery Cathodes. *Acc. Chem. Res.* **2012**, *46*, 1135−1143.

(7) Hendrickson, K. E.; Ma, L.; Cohn, G.; Lu, Y.; Archer, L. A. Model Membrane-Free Li−S Batteries for Enhanced Performance and Cycle Life. *Adv. Sci.* **2015**, *2*, 1500068.

(8) Manthiram, A.; Fu, Y.; Chung, S.-H.; Zu, C.; Su, Y.-S. Rechargeable Lithium−Sulfur Batteries. *Chem. Rev.* **2014**, *114*, 11751−11787.

DOI: 10.1021/acsnano.5b06373
ACS Nano 2016, 10, 1050−1059

(9) Zhang, S.; Ueno, K.; Dokko, K.; Watanabe, M. Recent Advances in Electrolytes for Lithium−Sulfur Batteries. *Adv. Energy Mater.* **2015**, *5*, 1500117.
(10) Schuster, J.; He, G.; Mandlmeier, B.; Yim, T.; Lee, K. T.; Bein, T.; Nazar, L. F. Spherical Ordered Mesoporous Carbon Nanoparticles with High Porosity for Lithium−Sulfur Batteries. *Angew. Chem., Int. Ed.* **2012**, *51*, 3591−3595.
(11) He, G.; Ji, X.; Nazar, L. High ″C″ Rate Li-S Cathodes: Sulfur Imbibed Bimodal Porous Carbons. *Energy Environ. Sci.* **2011**, *4*, 2878−2883.
(12) Zheng, G.; Yang, Y.; Cha, J. J.; Hong, S. S.; Cui, Y. Hollow Carbon Nanofiber-Encapsulated Sulfur Cathodes for High Specific Capacity Rechargeable Lithium Batteries. *Nano Lett.* **2011**, *11*, 4462−4467.
(13) Elazari, R.; Salitra, G.; Garsuch, A.; Panchenko, A.; Aurbach, D. Sulfur-Impregnated Activated Carbon Fiber Cloth as a Binder-Free Cathode for Rechargeable Li-S Batteries. *Adv. Mater.* **2011**, *23*, 5641−5644.
(14) Wang, H.; Yang, Y.; Liang, Y.; Robinson, J. T.; Li, Y.; Jackson, A.; Cui, Y.; Dai, H. Graphene-Wrapped Sulfur Particles as a Rechargeable Lithium-Sulfur Battery Cathode Material with High Capacity and Cycling stability. *Nano Lett.* **2011**, *11*, 2644−2647.
(15) Ji, L.; Rao, M.; Zheng, H.; Zhang, L.; Li, Y.; Duan, W.; Guo, J.; Cairns, E. J.; Zhang, Y. Graphene Oxide as a Sulfur Immobilizer in High Performance Lithium/Sulfur Cells. *J. Am. Chem. Soc.* **2011**, *133*, 18522−18525.
(16) Jayaprakash, N.; Shen, J.; Moganty, S. S.; Corona, A.; Archer, L. A. Porous Hollow Carbon@Sulfur Composites for High-Power Lithium−Sulfur Batteries. *Angew. Chem., Int. Ed.* **2011**, *50*, 5904−5908.
(17) Zhang, B.; Qin, X.; Li, G. R.; Gao, X. P. Enhancement of Long Stability of Sulfur Cathode by Encapsulating Sulfur into Micropores of Carbon Spheres. *Energy Environ. Sci.* **2010**, *3*, 1531.
(18) Guo, Y.-G.; Hu, J.-S.; Wan, L.-J. Nanostructured Materials for Electrochemical Energy Conversion and Storage Devices. *Adv. Mater.* **2008**, *20*, 2878−2887.
(19) Cheng, X.-B.; Huang, J.-Q.; Zhang, Q.; Peng, H.-J.; Zhao, M.-Q.; Wei, F. Aligned Carbon Nanotube/Sulfur Composite Cathodes with High Sulfur Content for Lithium−Sulfur Batteries. *Nano Energy* **2014**, *4*, 65−72.
(20) Zhou, G.; Wang, D.-W.; Li, F.; Hou, P.-X.; Yin, L.; Liu, C.; Lu, G. Q.; Gentle, I. R.; Cheng, H.-M. A Flexible Nanostructured Sulphur−Carbon Nanotube Cathode with High Rate Performance for Li-S Batteries. *Energy Environ. Sci.* **2012**, *5*, 8901.
(21) Ji, X.; Lee, K. T.; Nazar, L. F. A Highly Ordered Nanostructured Carbon-Sulphur Cathode for Lithium-Sulphur Batteries. *Nat. Mater.* **2009**, *8*, 500−506.
(22) Zhang, Q.; Huang, J. Q.; Qian, W. Z.; Zhang, Y. Y.; Wei, F. The Road for Nanomaterials Industry: a Review of Carbon Nanotube Production, Post-Treatment, and Bulk Applications for Composites and Energy Storage. *Small* **2013**, *9*, 1237−1265.
(23) Ji, X.; Evers, S.; Black, R.; Nazar, L. F. Stabilizing Lithium-Sulphur Cathodes Using Polysulphide Reservoirs. *Nat. Commun.* **2011**, *2*, 325.
(24) Evers, S.; Yim, T.; Nazar, L. F. Understanding the Nature of Absorption/Adsorption in Nanoporous Polysulfide Sorbents for the Li−S Battery. *J. Phys. Chem. C* **2012**, *116*, 19653−19658.
(25) Choi, Y. J.; Jung, B. S.; Lee, D. J.; Jeong, J. H.; Kim, K. W.; Ahn, H. J.; Cho, K. K.; Gu, H. B. Electrochemical Properties of Sulfur Electrode Containing Nano Al_2O_3 for Lithium/Sulfur Cell. *Phys. Scr.* **2007**, *T129*, 62−65.
(26) Ma, L.; Zhuang, H.; Lu, Y.; Moganty, S. S.; Hennig, R. G.; Archer, L. A. Tethered Molecular Sorbents: Enabling Metal-Sulfur Battery Cathodes. *Adv. Energy Mater.* **2014**, *4*, 1400390.
(27) Zhou, W.; Chen, H.; Yu, Y.; Wang, D.; Cui, Z.; DiSalvo, F. J.; Abruña, H. D. Amylopectin Wrapped Graphene Oxide/Sulfur for Improved Cyclability of Lithium−Sulfur Battery. *ACS Nano* **2013**, *7*, 8801−8808.
(28) Zheng, G.; Zhang, Q.; Cha, J. J.; Yang, Y.; Li, W.; Seh, Z. W.; Cui, Y. Amphiphilic Surface Modification of Hollow Carbon Nanofibers for Improved Cycle Life of Lithium Sulfur Batteries. *Nano Lett.* **2013**, *13*, 1265−1270.
(29) Meyer, B. Elemental Sulfur. *Chem. Rev.* **1976**, *76*, 367−388.
(30) WHITTINGHAM, M. S. Electrical Energy Storage and Intercalation Chemistry. *Science* **1976**, *192*, 1126−1127.
(31) Yi, C.; Qi, S.; Zhang, D.; Yang, M. Covalent Conjugation of Multi-Walled Carbon Nanotubes with Proteins. In *Carbon Nanotubes*; Balasubramanian, K.; Burghard, M., Eds.; Humana Press, 2010; Vol. *625*, pp 9−17.
(32) Kim, H. J.; Bae, I. S.; Cho, S. J.; Boo, J. H.; Lee, B. C.; Heo, J.; Chung, I.; Hong, B. Synthesis and Characteristics of NH2-Functionalized Polymer Films to Align and Immobilize DNA Molecules. *Nanoscale Res. Lett.* **2012**, *7*, 30.
(33) Ali, M. A.; Srivastava, S.; Solanki, P. R.; Reddy, V.; Agrawal, V. V.; Kim, C.; John, R.; Malhotra, B. D. Highly Efficient Bienzyme Functionalized Nanocomposite-Based Microfluidics Biosensor Platform for Biomedical Application. *Sci. Rep.* **2013**, *3*, 2661.
(34) Seh, Z. W.; Zhang, Q.; Li, W.; Zheng, G.; Yao, H.; Cui, Y. Stable Cycling of Lithium Sulfide Cathodes Through Strong Affinity with a Bifunctional Binder. *Chem. Sci.* **2013**, *4*, 3673−3677.
(35) Yoshida, T.; Sakakibara, K.; Asami, M.; Chen, K.-H.; Lii, J.-H.; Allinger, N. L. Molecular Mechanics (MM3) Calculations on Lithium Amide Compounds. *J. Comput. Chem.* **2003**, *24*, 319−327.
(36) Aurbach, D.; Pollak, E.; Elazari, R.; Salitra, G.; Kelley, C. S.; Affinito, J. On the Surface Chemical Aspects of Very High Energy Density, Rechargeable Li−Sulfur Batteries. *J. Electrochem. Soc.* **2009**, *156*, A694.
(37) Hampton, M. A.; Plackowski, C.; Nguyen, A. V. Physical and Chemical Analysis of Elemental Sulfur Formation during Galena Surface Oxidation. *Langmuir* **2011**, *27*, 4190−4201.
(38) Liang, X.; Hart, C.; Pang, Q.; Garsuch, A.; Weiss, T.; Nazar, L. F. A Highly Efficient Polysulfide Mediator for Lithium−Sulfur Batteries. *Nat. Commun.* **2015**, *6*, 5682.
(39) Wang, Z.; Dong, Y.; Li, H.; Zhao, Z.; Wu, H. B.; Hao, C.; Liu, S.; Qiu, J.; Lou, X. W. Enhancing Lithium-Sulphur Battery Performance by Strongly Binding the Discharge Products on Amino-Functionalized Reduced Graphene Oxide. *Nat. Commun.* **2014**, *5*, 5002.
(40) Thomson, J. W.; Nagashima, K.; Macdonald, P. M.; Ozin, G. A. From Sulfur-Amine Solutions to Metal Sulfide Nanocrystals: Peering into the Oleylamine-Sulfur Black Box. *J. Am. Chem. Soc.* **2011**, *133*, 5036−5041.
(41) Davis, R. E.; Nakshbendi, H. F. Sulfur in Amine Solvents. *J. Am. Chem. Soc.* **1962**, *84*, 2085−2090.
(42) Jimeno, A.; Goyanes, S.; Eceiza, A.; Kortaberria, G.; Mondragon, I.; Corcuera, M. A. Effects of Amine Molecular Structure on Carbon Nanotubes Functionalization. *J. Nanosci. Nanotechnol.* **2009**, *9*, 6222−6227.
(43) Kim, J. H.; Kim, T.; Jeong, Y. C.; Lee, K.; Park, K. T.; Yang, S. J.; Park, C. R. Stabilization of Insoluble Discharge Products by Facile Aniline Modification for High Performance Li-S Batteries. *Adv. Energy Mater.* **2015**, *5*, 1500268.
(44) Rauh, R. D.; Abraham, K. M.; Pearson, G. F.; Surprenant, J. K.; Brummer, S. B. A Lithium/Dissolved Sulfur Battery with an Organic Electrolyte. *J. Electrochem. Soc.* **1979**, *126*, 523−527.
(45) Frisch, M. J.; Trucks, G. W.; Schlegel, H. B.; Scuseria, G. E.; Robb, M. A.; Cheeseman, J. R.; Scalmani, G.; Barone, V.; Mennucci, B.; Petersson, G. A.; Nakatsuji, H.; et al. *Gaussian 09*, Gaussian, Inc.: Wallingford, CT, USA, 2009.

DOI: 10.1021/acsnano.5b06373
ACS Nano 2016, 10, 1050−1059